RSC Advances

ROYAL SOCIETY OF CHEMISTRY

www.rsc.org/advances

Diorganotin(IV) 4,6-dimethyl-2-pyrimidyl selenolates: Synthesis, structures and their utility as molecular precursors for the preparation of $SnSe_2$ nano-sheets and thin films

Adish Tyagi,[a] G. Kedarnath,*[a] Amey Wadawale,[a] Alpa Y. Shah,[a] Vimal K. Jain*[a] and B. Vishwanadh[b]

[a]*Chemistry Division, Bhabha Atomic Research Centre, Mumbai- 400 085 (India),*
Email: kedar@barc.gov.in; jainvk@barc.gov.in
[b]*Materials Science Division, Bhabha Atomic Research Centre, Mumbai- 400 085 (India),*

The complexes of composition, $[R_2Sn\{SeC_4H(Me\text{-}4,6)_2N_2\}_2]$ (R = Me, Et, ^{n}Bu or ^{t}Bu) have been isolated by the reaction of R_2SnCl_2 with $NaSeC_4H(Me\text{-}4,6)_2N_2$. The treatment of $[R_2Sn\{SeC_4H(Me\text{-}4,6)_2N_2\}_2]$ with R_2SnCl_2 afforded chloro complexes, $[R_2SnCl\{SeC_4H(Me\text{-}4,6)_2N_2\}]$ (R = Me, ^{n}Bu or ^{t}Bu). These complexes were characterized by elemental analyses, and NMR (^{1}H, ^{13}C, ^{77}Se, ^{119}Sn) spectroscopy. The molecular structures of $[^tBu_2Sn\{SeC_4H(Me\text{-}4,6)_2N_2\}_2]$ and $[^tBu_2SnCl\{SeC_4H(Me\text{-}4,6)_2N_2\}]$ were established by single crystal X- ray diffraction analyses. Thermolysis of $[R_2Sn\{SeC_4H(Me\text{-}4,6)_2N_2\}_2]$ (R = Et, ^{n}Bu or ^{t}Bu) in oleylamine (OLA) afforded nanocrystalline hexagonal phase of $SnSe_2$. Thin films of $SnSe_2$ were deposited on silicon wafers by AACVD of $[^tBu_2Sn\{SeC_4H(Me\text{-}4,6)_2N_2\}_2]$. The nanostructures and thin films were characterized by solid state diffuse reflectance spectroscopy, XRD, EDX, SEM and TEM techniques. The solid state diffuse reflectance measurements of the nanosheets showed direct and indirect band gaps in the ranges of 1.76 – 2.30 eV and 1.38 – 1.49 eV, respectively which are blue shifted relative to bulk tin selenide.

Keywords: Diorganotin complexes, 2-Pyrimidylselenolate, Tin selenide, nanostructures, Thin films, NMR, X-ray structure

Introduction

Interest in tin chalcogenide semiconductor materials is growing rapidly due to their desirable electronic and optical properties which make them promising candidates for photovoltaic devices[1-5]. They are also emerging as alternatives to other chalcogenide materials like PbE, CdE, $CuInE_2$ (E = S, Se, Te), etc; due to their higher carrier mobility, lower toxicity as well as lower cost[6,7].

Among tin chalcogenides, tin selenides have received considerable attention in recent years. Tin selenides exist in two stoichiometric narrow direct band phases, i.e. orthorhombic SnSe (band gap ~ 1.0 eV) and hexagonal $SnSe_2$ (band gap ~ 0.9 eV) and adopt layered structures at room temperature[5,8]. Anistropic properties of the SnSe have been exploited for thermoelectric and photovoltaic applications[8, 9]; whereas the composites of two dimensional layered $SnSe_2$ with graphene have been used as an anode material for lithium ion batteries[5].

Several synthetic approaches have been adopted for the preparation of tin selenide nano-structures and for deposition of thin films. Usually $SnCl_2$ and suitable selenium source (e.g., R_2Se, TOP-Se, etc.) are employed to prepare SnSe[10,11] and $SnSe_2$ [5,10,12]. Single source molecular precursor (ssp) strategy is a versatile material growth process. It has been successfully employed for the preparation of variety of nanomaterials and also for the deposition of thin films. This route has met with a little success in the case of tin selenide possibly due to limited exploration of tin complexes with selenium ligands as ssp. Boudjouk and co-workers used benzyltin [e.g., $(Bz_2SnE)_3$, $(Bz_3Sn)_2E$][13] and phenyl tin [e.g., $(Ph_3Sn)_2E$, where E = S, Se, Te][14,15] chalcogenides for the synthesis of tin chalcogenides, but the resulting materials were often contaminated with elemental tin[15]. The complex $[Sn\{CH(SiMe_3)_2\}_2(\mu\text{-}Se)]_2$ has been employed for deposition of thin films of SnSe by MOCVD[16], whereas $[Sn(SeC_5H_4N)_2]_2$ could not be used for deposition of thin films due to low volatility of the complex, although it yielded SnSe on thermolysis[17]. The ssp for $SnSe_2$ are rather rare. The bulk thermolysis of $[Sn(SeC_5H_4N)_4]$ yields $SnSe_2$ [17]. Recently we have reported diorganotin 2-pyridylselenolate complexes which on thermolysis in coordinating solvents afforded SnSe and $SnSe_2$ depending on the pyrolysis condition[18] whereas the complex, $[^tBu_2Sn(SeC_5H_4N)_2]$ could deposit thin films of only SnSe[18]. The higher deposition temperature of these complexes has led to vaporization of selenium giving SnSe and in some cases a mixture of SnSe and $SnSe_2$. The lower deposition temperature precursors are likely to afford $SnSe_2$ which could be accomplished with the 2-pyrimidyl selenolates of diorganotin(IV).

Herein we describe the synthesis of a new series of diorganotin precursors derived from 4,6-dimethyl-2-pyrimidyl selenolate which served the dual purpose of synthesis of $SnSe_2$ nanosheets as well as precursors for deposition of $SnSe_2$ thin films.

Experimental

Materials and Methods

Diorganotin chlorides (R_2SnCl_2; R = Me, Et, ^nBu or ^tBu), oleylamine (OLA) and analytical grade solvents were obtained from commercial sources. The diselenide, $[SeC_4H(Me\text{-}4,6)_2N_2]_2$ (^1H NMR

($CDCl_3$) δ: 2.37 (s, Me); 6.71 (s, CH-5) . $^{13}C\{^1H\}$ NMR ($CDCl_3$) δ: 23.7 (Me); 117.2 (CH-5); 165.7 (C-2); 167.5 (C-4,6). $^{77}Se\{^1H\}$ NMR ($CDCl_3$) δ: 486 ppm) was prepared according to literature method[19].

Elemental analyses were carried out on a Thermo Fischer Flash EA-1112 CHNS analyzer. The ^1H, $^{13}C\{^1H\}$, $^{77}Se\{^1H\}$ and $^{119}Sn\{^1H\}$ NMR spectra were recorded on a Bruker Avance-II NMR spectrometer operating at 300, 75.47, 57.24 and 111.92 MHz, respectively. Chemical shifts are relative to internal chloroform peak for ^1H and $^{13}C\{^1H\}$ NMR spectra, external Ph_2Se_2 (δ 463 ppm relative to Me_2Se) in $CDCl_3$ for $^{77}Se\{^1H\}$ and 30% Me_4Sn in C_6D_6 for $^{119}Sn\{^1H\}$ NMR spectra. Optical diffuse reflectance measurements in the range 200−1800 nm (0.68 eV to 6.2 eV) were performed on a JASCO V-670 two-beam spectrometer with a diffuse reflectance (DR) attachment consisting of an integration sphere coated with barium sulfate which was used as a reference material. Measured reflectance data were converted to absorption (A) using Kubelka-Munk remission function[20]. The band gaps of the samples were estimated by extrapolating the linear portion of the plot to X (energy) axis.

Thermogravimetric analyses (TGA) were carried out on a Nitzsch STA 409 PC-Luxx TG-DTA instrument, which was calibrated with $CaC_2O_4.H_2O$. The TG curves were recorded at a heating rate of 10 $^oC\ min^{-1}$ under a flow of argon. X-ray powder diffraction patterns were obtained on a Philips PW-1820 diffractometer using CuK_α radiation. SEM and EDX measurements were carried out on ULTRA 55 FESEM of Zeiss and Oxford Inca instruments, respectively. Tecnai G2 T20 transmission electron microscopes operating at accelerating voltages up to 200 kV were used for TEM studies. The samples for TEM and SAED were prepared by placing a drop of sample dispersed in acetone/toluene on a carbon coated copper grid.

Intensity data for [$^nBu_2Sn\{SeC_4H(Me\text{-}4,6)_2N_2\}_2$] (**3**) [$^tBu_2Sn\{SeC_4H(Me\text{-}4,6)_2N_2\}_2$] (**4**) and [$^tBu_2Sn\{SeC_4H(Me\text{-}4,6)_2N_2\}Cl$] (**7**) were collected at room temperature (298 ± 2K) on a Rigaku AFC7S diffractometer using graphite monochromated Mo K_α (λ = 0.71069 Å) radiation so that θ_{max} = 27.5°. The unit cell parameters (Table 1) were determined from 25 reflections measured by a random search routine. The intensity data were corrected for Lorentz, polarization and absorption effects with an empirical procedure.[21] The structures were solved by direct methods using SHELX-97[22] and refined by full-matrix least squares methods. The non-hydrogen atoms were refined anisotropically. The hydrogen atoms were fixed in their calculated positions. Molecular structures were drawn using ORTEP.[23]

Syntheses of complexes

[$Me_2Sn\{SeC_4H(Me\text{-}4,6)_2N_2\}_2$] (1)

To a freshly prepared solution of $NaSeC_4H(Me\text{-}4,6)_2N_2$ [obtained by the reduction of $\{SeC_4H(Me\text{-}4,6)_2N_2\}_2$ (191 mg, 0.51 mmol) in toluene with methanolic $NaBH_4$ (39 mg, 1.30 mmol)], solid Me_2SnCl_2 (112 mg, 0.51 mmol) was added with vigorous stirring which continued for 3 h at room temperature. The solvents were evaporated under vacuum and the residue was washed thoroughly with toluene-hexane mixture (1:20 v/v). The pure product was extracted with chloroform and filtered to remove NaCl. The filtrate was dried under reduced pressure and recrystallized from toluene-dichloromethane mixture to give a white powder (yield: 160 mg, 60%), mp 163 ^oC. Anal. Calcd. for $C_{14}H_{20}N_4Se_2Sn$: C, 32.28; H, 3.87; N 10.75%. Found: C, 32.15; H, 3.81; N, 10.51%. ^1H NMR ($CDCl_3$) δ: 1.12 (s, Me_2Sn, 6 H, $^2J(^{119}Sn\text{-}^1H)$ = 72 Hz; $^2J(^{117}Sn\text{-}^1H)$ = 69 Hz); 2.36 (s, $C_4H(Me\text{-}4,6)N_2$, 12 H); 6.74 (s, C*H*-5, $C_4H(Me\text{-}4,6)N_2$). $^{13}C\{^1H\}$ NMR ($CDCl_3$) δ: 4.8 ($SnCH_3$, $^1J(^{119}Sn\text{-}^{13}C)$ = 527 Hz; $^1J(^{117}Sn\text{-}^{13}C)$ = 503 Hz), 23.3 ($C_4H(Me\text{-}4,6)N_2$), 115.7 (C-5), 166.4 (C-4,6), 169.81 (C-Se). $^{77}Se\{^1H\}$ NMR ($CDCl_3$) δ: 233 ($^1J(^{119}Sn\text{-}^{77}Se)$ = 725 Hz; $^1J(^{117}Sn\text{-}^{77}Se)$ = 692 Hz). $^{119}Sn\{^1H\}$ NMR ($CDCl_3$) δ: −135 (^1J(Sn-Se) = 724 Hz) ppm.

[$Et_2Sn\{SeC_4H(Me\text{-}4,6)_2N_2\}_2$] (2)

Prepared similar to **1** and recrystallized from toluene-dichloromethane mixture as colorless crystals in 70% yield, mp 146 ^oC. Anal. Calcd. for $C_{16}H_{24}N_4Se_2Sn$: C, 35.00; H, 4.41; N 10.20%. Found: C, 34.72; H, 4.37; N 10.06%. ^1H NMR ($CDCl_3$) δ: 1.26 (t, $SnCH_2CH_3$, 6 H, 7.8 Hz); 1.68 (q, $SnCH_2CH_3$, 4 H); 2.36 (s, $C_4H(Me\text{-}4,6)N_2$, 12 H); 6.73 (s, C*H*-5, $C_4H(Me\text{-}4,6)N_2$). $^{13}C\{^1H\}$ NMR ($CDCl_3$) δ: 11.0 ($SnCH_2CH_3$, $^2J(^{119}Sn\text{-}^{13}C)$ = 40 Hz), 16.3 ($SnCH_2CH_3$, $^1J(^{119}Sn\text{-}^{13}C)$ = 502 Hz; $^1J(^{117}Sn\text{-}^{13}C)$ = 481 Hz), 23.5 ($C_4H(Me\text{-}4,6)N_2$), 115.7 (C-5), 166.4 (C-4,6), 170.7 (C-Se). $^{77}Se\{^1H\}$ NMR ($CDCl_3$) δ: 180 ($^1J(^{119}Sn\text{-}^{77}Se)$ = 723 Hz; $^1J(^{117}Sn\text{-}^{77}Se)$ = 690 Hz). $^{119}Sn\{^1H\}$ NMR ($CDCl_3$) δ: −87 ($^1J(^{119}Sn\text{-}^{77}Se)$ = 726 Hz) ppm.

[$^nBu_2Sn\{SeC_4H(Me\text{-}4,6)_2N_2\}_2$] (3)

Prepared in a similar fashion to **1** and recrystallized from toluene-dichloromethane mixture as colorless crystals in 66% yield, mp 126 ^oC. Anal. Calcd. for $C_{20}H_{32}N_4Se_2Sn$: C, 39.69; H, 5.33, N, 9.26%. Found: C, 39.31; H, 5.23; N, 9.13%. ^1H NMR ($CDCl_3$) δ: 0.79 (t, $SnCH_2CH_2CH_2CH_3$, 6 H, 7.2 Hz); 1.33 (m), 1.58-1.75 (m) (SnBu); 2.37 (s, $C_4H(Me\text{-}4,6)N_2$, 12 H); 6.74 (s, C*H*-5, $C_4H(Me\text{-}4,6)N_2$). $^{13}C\{^1H\}$ NMR ($CDCl_3$) δ: 13.6 ($SnCH_2CH_2CH_2CH_3$), 23.1 ($SnCH_2CH_2CH_2CH_3$, $^1J(^{119}Sn\text{-}^{13}C)$ = 479 Hz; $^1J(^{117}Sn\text{-}^{13}C)$ = 458 Hz), 23.6 ($C_4H(Me\text{-}4,6)N_2$), 26.3 ($SnCH_2CH_2CH_2CH_3$, $^2J(^{119}Sn\text{-}^{13}C)$ = 99 Hz), 28.7 ($SnCH_2CH_2CH_2CH_3$, $^3J(^{119}Sn\text{-}^{13}C)$ = 35 Hz), 115.8 (C-5), 166.5 (C-4,6), 170.6 (C-Se). $^{77}Se\{^1H\}$ NMR

($CDCl_3$) δ: 194 ($^1J(^{119}Sn\text{-}^{77}Se)$ = 745 Hz; $^1J(^{117}Sn\text{-}^{77}Se)$ = 711 Hz). $^{119}Sn\{^1H\}$ NMR ($CDCl_3$) δ: –92 ($^1J(^{119}Sn\text{-}^{77}Se)$ = 746 Hz) ppm.

[^{t}Bu$_2$Sn{SeC$_4$H(Me-4,6)$_2$N$_2$}$_2$] (4)

Prepared similar to **1** and recrystallized from toluene-dichloromethane as colorless crystals in 68% yield, mp 157 ^{o}C. Anal. Calcd. for $C_{20}H_{32}N_4Se_2Sn$: C, 39.69; H, 5.33; N, 9.26%. Found: C, 39.38; H, 5.26; N, 9.40%. ^1H NMR ($CDCl_3$) δ: 1.48 (s, ^{t}Bu$_2$Sn, 18 H, ^3J (Sn-H) = 99 Hz); 2.37 (s, C$_4$H(*Me*-4,6)N$_2$, 12 H); 6.70 (s, C*H*-5, C$_4$H(Me-4,6)N$_2$). $^{13}C\{^1H\}$ NMR ($CDCl_3$) δ: 23.7 (C$_4$H(*Me*-4,6)N$_2$), 31.9 (Me$_3$C-Sn), 41.6 (C-Sn), 116.4 (C-5), 166.6 (C-4,6), 170.3 (C-Se). $^{77}Se\{^1H\}$ NMR ($CDCl_3$) δ: 182 (^1J(Sn-Se) = 977 Hz). $^{119}Sn\{^1H\}$ NMR ($CDCl_3$) δ: 28 ($^1J(^{119}Sn\text{-}^{77}Se)$ = 999 Hz) ppm.

[Me$_2$SnCl{SeC$_4$H(Me-4,6)$_2$N$_2$}] (5)

To a toluene solution of [Me$_2$Sn{SeC$_4$H(Me-4,6)$_2$N$_2$}$_2$] (100 mg, 0.192 mmol), Me$_2$SnCl$_2$ (42 mg, 0.191 mmol) solution in the same solvent was added and the whole mixture was stirred at room temperature for 1 h. The solvents were evaporated under vacuum to yield a solid (yield: 61.26 mg, 86%), mp 108 ^{o}C. Anal. Calcd. for $C_8H_{13}N_2ClSeSn$: C, 25.95; H, 3.54; N, 7.56%. Found: C, 25.76; H, 3.63; N, 7.41%. ^1H NMR ($CDCl_3$) δ: 1.14 (s, Me$_2$Sn, 6 H, ^2J(Sn–H) = 71 Hz); 2.35 (s, C$_4$H(*Me*-4,6)N$_2$, 6 H); 6.84 (s, C*H*-5, C$_4$H(Me-4,6)N$_2$). $^{13}C\{^1H\}$ NMR ($CDCl_3$) δ: 5.6 (Sn*CH$_3$*, $^1J(^{119}Sn\text{-}^{13}C)$ = 532 Hz; $^1J(^{117}Sn\text{-}^{13}C)$ = 509 Hz), 23.0 (C$_4$H(*Me*-4,6)N$_2$), 116.5 (C-5), 167.1 (C-4,6), 170.4 (C-Se). $^{77}Se\{^1H\}$ NMR ($CDCl_3$) δ: 262 (^1J(Sn -Se) = 724 Hz). $^{119}Sn\{^1H\}$ NMR ($CDCl_3$) δ: –90 ($^1J(^{119}Sn\text{-}^{77}Se)$ = 727 Hz) ppm.

[^{n}Bu$_2$SnCl{SeC$_4$H(Me-4,6)$_2$N$_2$}] (6)

Prepared in a similar fashion to **5** and the complex was extracted with hexane and dried under vacuum to give a colorless liquid in 71% yield. Anal. Calcd. for $C_{14}H_{25}N_2ClSeSn$: C, 37.00; H, 5.54; N, 6.16%. Found: C, 36.67; H, 5.41; N, 6.05%. ^1H NMR ($CDCl_3$) δ: 0.89 (t, SnCH$_2$CH$_2$CH$_2$C*H$_3$*, 6 H, 7.2 Hz); 1.37 (m), 1.69-1.77 (m) (SnBu); 2.35 (s, C$_4$H(*Me*-4,6)N$_2$, 6 H); 6.84 (s, C*H*-5, C$_4$H(Me-4,6)N$_2$). $^{13}C\{^1H\}$ NMR ($CDCl_3$) δ: 13.6 (SnCH$_2$CH$_2$CH$_2$*CH$_3$*,), 24.6 (Sn*C*H$_2$CH$_2$CH$_2$CH$_3$, $^1J(^{119}Sn\text{-}^{13}C)$ = 486 Hz; $^1J(^{117}Sn\text{-}^{13}C)$ = 465 Hz), 23.2 (C$_4$H(*Me*-4,6)N$_2$), 26.2 (SnCH$_2$*C*H$_2$CH$_2$CH$_3$, $^2J(^{119}Sn\text{-}^{13}C)$ = 90 Hz), 27.8 (SnCH$_2$CH$_2$*C*H$_2$CH$_3$, $^3J(^{119}Sn\text{-}^{13}C)$ = 35 Hz), 116.7 (C-5), 167.2 (C-4,6), 170.7 (C-Se). $^{77}Se\{^1H\}$ NMR ($CDCl_3$) δ: 228 ($^1J(^{119}Sn\text{-}^{77}Se)$ = 748 Hz; $^1J(^{117}Sn\text{-}^{77}Se)$ = 713 Hz). $^{119}Sn\{^1H\}$ NMR ($CDCl_3$) δ: –74 ($^1J(^{119}Sn\text{-}^{77}Se)$ = 755 Hz) ppm.

[$^{t}Bu_2SnCl\{SeC_4H(Me\text{-}4,6)_2N_2\}$] (7)

Prepared in a similar fashion to **5** and recrystallized from dichloromethane-hexane as colorless crystals in 82% yield, mp 101 ^{o}C. Anal. Calcd. for $C_{14}H_{25}N_2ClSeSn$: C, 36.99; H, 5.54; N, 6.16%. Found: C, 36.81; H, 5.51; N, 5.98%. ^{1}H NMR ($CDCl_3$) δ: 1.48 (s, $^{t}Bu_2Sn$, 18 H, $^{3}J(^{119}Sn\text{-}^{1}H)$ = 110 Hz; $^{3}J(^{117}Sn\text{-}^{1}H)$ = 108 Hz); 2.38 (s, $C_4H(Me\text{-}4,6)N_2$, 6 H); 6.81 (s, C*H*-5, $C_4H(Me\text{-}4,6)N_2$). $^{13}C\{^{1}H\}$ NMR ($CDCl_3$) δ: 23.9 ($C_4H(Me\text{-}4,6)N_2$), 30.9 (Me_3C-Sn), 43.4 (C-Sn, $^{1}J(^{119}Sn\text{-}^{13}C)$ = 398 Hz; $^{1}J(^{117}Sn\text{-}^{13}C)$ = 380 Hz), 117.0 (C-5), 167.0 (C-4,6), 171.5 (C-Se). $^{77}Se\{^{1}H\}$ NMR ($CDCl_3$) δ: 197 ($^{1}J(^{119}Sn\text{-}^{77}Se)$ = 910 Hz; $^{1}J(^{117}Sn\text{-}^{77}Se)$ = 870 Hz). $^{119}Sn\{^{1}H\}$ NMR ($CDCl_3$) δ: –20 (^{1}J(Sn-Se) = 912 Hz) ppm.

Preparation of tin selenide nanoparticles

In a typical experiment, an OLA (2 ml) dispersion of complex **2** (100 mg, 0.18 mmol), **3** (100 mg, 0.17 mmol) or **4** (100 mg, 0.17 mmol) was injected rapidly into a preheated (210 ^{o}C) OLA (8 ml) in a three-necked flask with vigorous stirring under flowing argon. The temperature of the reaction mixture was dropped in the range of ~185 °C upon injection which again raised to 210 ^{o}C. The reaction mixture was kept at 210 ^{o}C for different durations (2, 5 and 10 minutes). After the desired growth time, the reaction mixture was cooled down rapidly to 95-98 °C and quenched by injecting toluene (4 ml). The resulting nanocrystals were separated by precipitating with excess methanol followed by centrifugation to give a black powder.

Preparation of thin films by Aerosol Assisted Chemical Vapor Deposition (AACVD)

A toluene solution (25 ml) of **4** (125 mg, 0.21 mmol) was used to generate aerosol by an ultrasonic humidifier. The aerosol was transported over a period of 1 h using argon as a carrier gas (flow rates of 180 sccm) to a preheated silicon wafer (110) orientation placed in a turbo furnace at 375 ^{o}C.

Results and discussion

Synthesis and Spectroscopy

Treatment of R_2SnCl_2 (R = Me, Et, ^{n}Bu, ^{t}Bu) with two equivalents of sodium 4,6-dimethyl-2-pyrimidyl selenolate, $NaSeC_4H(Me\text{-}4,6)_2N_2$, in a toluene-methanol mixture gave diorganotin selenolate complexes, $[R_2Sn\{SeC_4H(Me\text{-}4,6)_2N_2\}_2]$ (R = Me (**1**), Et (**2**), ^{n}Bu (**3**), ^{t}Bu (**4**)) (Scheme 1). The latter when treated with an equivalent of R_2SnCl_2 in toluene mixture gave chloro complexes, $[R_2SnCl\{SeC_4H(Me\text{-}4,6)_2N_2\}]$ (R = Me (**5**), ^{n}Bu (**6**), ^{t}Bu (**7**)).

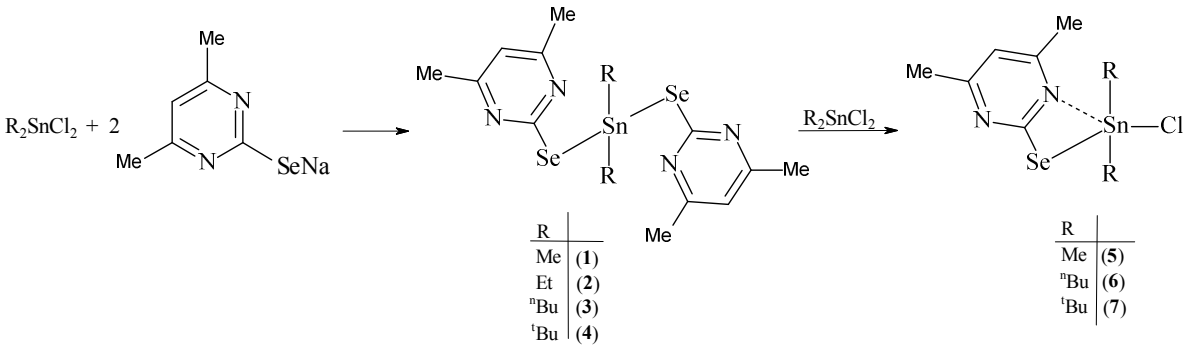

Scheme 1. Synthesis of organotin selenolate complexes

The ^{1}H, $^{13}C\{^{1}H\}$, $^{77}Se\{^{1}H\}$ and $^{119}Sn\{^{1}H\}$ NMR spectra were recorded in $CDCl_3$ (Supplementary information). ^{1}H and ^{13}C NMR spectra showed expected resonances and peak multiplicities. The pyrimidyl ring proton resonances shifted to down field with reference to the corresponding signals for the diselenides. The magnitudes of $^{1}J(^{119}Sn–^{13}C)$ and $^{2}J(^{119}Sn–^{1}H)$ for dimethyltin complexes (**1** and **5**) are similar to other dimethyltin(IV) derivatives with thio-/seleno-pyridine ligands[18, 24]. ^{1}J(Sn-C) values decreases gradually on replacing methyl groups attached to tin by Et, ^{n}Bu or ^{t}Bu which may be due to the increasing steric hindrance resulting in diminishing the electron acceptor property of tin.[18,25] This effect is further corroborated by larger Sn-C bond length in $[^{t}Bu_2Sn(2\text{-}SeC_5H_4N)_2]$ as compared to its methyl analogue[18].

The $^{77}Se\{^{1}H\}$ NMR spectra displayed single resonances (range 170-262 ppm) which were flanked by ^{119}Sn and ^{117}Sn satellites with the coupling constants in the range 723-977 Hz. The magnitude of $^{1}J(^{119}Sn–^{77}Se)$ coupling constant is higher than the analogous complexes derived 2-pyridine selenolate ligand, $[R'_2Sn(SeC_5H_3R\text{-}3)_2]$ (R = H or Me) and $[R'_2SnCl\{SeC_5H_3(R\text{-}3)\}]$[18]. This indicates stronger Sn-Se bonding in these complexes than the 2-pyridine selenolate derivatives which is reflected from the Sn-Se bond distances determined from X-ray analysis (see later). The resonance within the series (bis or chloro) is shielded on replacing methyl groups on tin by Et, ^{n}Bu or ^{t}Bu groups which could be due to +I effect of the larger alkyl group. Similarly, ^{77}Se signal of **4** is shielded relative to that of **3** as +I effect is more pronounced in branched chain alkyl groups compared to the straight chain alkyl groups with same number of carbons. The ^{77}Se resonance for chloro derivatives (**5-7**) are deshielded (~30-20 ppm) with respect to the corresponding bis complexes.

In contrast to ^{1}J(Sn-C),^{1}J(Sn-Se) values gradually increase with increasing carbon chain length of the alkyl group which may be due to increased inductive effect (+I). The +I effect increases the electron density on tin atom results in better overlapping of tin and selenium molecular orbitals. Among $[^{n}Bu_2Sn\{SeC_4H(Me\text{-}4,6)_2N_2\}_2]$ (**3**) and its ^{t}Bu- analogue (**4**), the latter has higher ^{1}J(Sn-Se) value

compared to the former. This is due to relatively stronger +I effect in case of branched chain alkyl groups than straighter one with the same number of carbon atoms. Corresponding chloro derivatives show smaller coupling constant of (Sn-Se) than the bis complexes. This may be due to –I effect of Cl attached to Sn which reduces the electron density on tin leading to decreased orbital overlap between tin and selenium.

The $^{119}Sn\{^{1}H\}$ NMR spectra showed single resonances in the range –135 to 28 ppm with $^{1}J(^{119}Sn–^{77}Se)$ couplings varying between 724 and 999 Hz . These resonances are deshielded with reference to the ^{119}Sn NMR signal for the corresponding 2-pyridylselenolate complexes indicating weaker Sn...N interactions in the former. The resonance within the series (bis or chloro) is deshielded on replacing methyl groups on tin by Et, ^{n}Bu or ^{t}Bu groups which could be due to +I effect of the larger alkyl group, and is in conformity with the trend noted for diorgaotin dichlorides (e.g., R_2SnCl_2; R/δ ^{119}Sn (in ppm) = Me/141; Et/126; ^{n}Bu/122; ^{t}Bu/52)[26]. The variable temperature ^{119}Sn NMR spectra of **7** were recorded in methanol-d_4 to assess whether there is any interaction between tin and nitrogen. There was a slight shift in the ^{119}Sn NMR resonance on lowering the temperature from RT to -40°C (^{119}Sn NMR δ: -18 at RT and -22 ppm at -40°C) (Supplementary information) indicating that there is no change in the coordination around tin. Temperature dependent ^{119}Sn NMR chemical shifts of diorganotin carboxylates have been attributed to change in the coordination environment around tin[27].

X-ray Crystallography

The molecular structures of $[^{t}Bu_2Sn\{SeC_4H(Me\text{-}4,6)_2N_2\}_2]$ (**4**) and $[^{t}Bu_2Sn\{SeC_4H(Me\text{-}4,6)_2N_2\}Cl]$ (**7**) with atomic numbering scheme are shown in Figures 1 and 2. Selected inter-atomic parameters are given in Tables 2 and 3. Both the complexes are discrete monomers, but differ in the coordination geometry around tin.

The coordination geometry around tin in $[^{t}Bu_2Sn\{SeC_4H(Me\text{-}4,6)_2N_2\}_2]$ (**4**) can be defined by carbon atoms of two ^{t}Bu groups and selenium from monodentate 2-pyrimidylselenolate ligands. The Sn…N distances are longer than the sum of their covalent radii (2.15 Å) but are shorter than the sum of van der Waal's radii (3.72 Å). The Sn…N separation in the present case is longer than the one reported in $[^{t}Bu_2Sn(SeC_5H_4N)_2]$ (Sn…N = 2.425(9) Å)[18]. A similar structure is observed for $[^{n}Bu_2Sn\{SeC_4H(Me\text{-}4,6)_2N_2\}_2]$ (**3**) but due to high R factor, the structure and data are included in supplementary information (Figure S1, Tables S1 and S2). The Sn–Se bond distance (2.5800(6) is shorter than those reported in $[Sn(SeC_5H_4N)_2]_2$ (2.681, 2.759 Å)[17], $_{\infty}{}^{1}[Sn(SePh)_2]$ (2.668, 2.675, 2.683, 2.673 Å)[28] and $[^{t}Bu_2Sn(2\text{-}SeC_5H_4N)_2]$[18] (2.622(2) Å). The Se–Sn–Se angle (86.19(3)^{o}) is contracted by 3^{o} to that of $[^{t}Bu_2Sn(2\text{-}$

$SeC_5H_4N)_2$] (89.14(11)°)[18] and [$^nBu_2Sn\{SC_5H_3N(5\text{-}NO_2)\}_2$] (89.9(1)°)[29]. The Sn–C_{butyl} bond distance (2.205(4) Å) is slightly shorter than that of [$^tBu_2Sn(2\text{-}SeC_5H_4N)_2$] (2.246(10) Å) while it is comparable to the value reported for [$^tBu_2Sn(\mu\text{-}OH)\{O(S)P(OEt_2)_2\}]_2$ (av. 2.16 Å)[30].

The tin in [$^tBu_2SnCl\{SeC_4H(Me\text{-}4,6)_2N_2\}$] (**7**) acquires a distorted trigonal bipyramidyl geometry defined by a Cl, two $^tBu_2$ and Se, N of a selenopyrimidine ligand where the chloride atom and chelating pyrimidylselenolate occupy the equatorial plane while two *tert*-butyl groups are directed axially. The Sn…N distance (2.784 Å) is shorter than the sum of their van der Waals radii[31]. The Sn–N (2.784 Å) separation is larger than the one reported in [$Me_2SnCl(SepyMe)$] (2.425(9) Å),[18] [$Ph_2SnCl(SC_5H_4N)$] (2.413 Å)[32] and [$R_2SnCl\{SC_4H(Me\text{-}4,6)_2N_2\}$] (R = Me or Et) (~2.51 Å)[24] but is comparable to [$^tBu_2Sn(2\text{-}SeC_5H_4N)_2$] (2.827 Å)[18] and [$(c\text{-}Hex)_2Sn(SC_5H_4N)_2$] (2.72 Å)[33]. The Sn–Cl bond distance (2.418(3) Å) is as expected and is comparable to the values reported for [$Ph_2SnCl(SC_5H_4N)$] (2.45 Å)[29] and [$SnCl_4(Et_2Se)_2$] (2.42, 2.43 Å)[34].

Thermal studies

Thermo gravimetric analyses (TGA) (Supplementary information Figures S2 - S6) of these complexes were performed under a flowing argon atmosphere. The bis complexes, [$R_2Sn\{SeC_4H(Me\text{-}4,6)_2N_2\}_2$] underwent a single step decomposition. From the weight loss in the TG pattern it can be inferred that the complexes [$Me_2Sn\{SeC_4H(Me\text{-}4,6)_2N_2\}_2$] (weight loss: found 62.0%, calcd. 58.8%) and [$^tBu_2Sn\{SeC_4H(Me\text{-}4,6)_2N_2\}_2$] (weight loss: found 68.0%, calcd. 67.3%) gave SnSe whereas [$Et_2Sn\{SeC_4H(Me\text{-}4,6)_2N_2\}_2$] (weight loss: found 54.8%, calcd. 49.6%) and [$^nBu_2Sn\{SeC_4H(Me\text{-}4,6)_2N_2\}_2$] (weight loss: found 54.5%, calcd. 54.3%) afforded $SnSe_2$. The %weight loss of **2** is higher than expected for the formation of $SnSe_2$ which may be due to partial sublimation during major weight loss step prior to the formation of $SnSe_2$.[35] The complex, [$^tBu_2Sn\{SeC_4H(Me\text{-}4,6)_2N_2\}Cl$] (7) underwent decomposition via two overlapping steps leading to the formation of tin (weight loss: found 71.2%, calcd. 73.8%). The first step corresponds to the formation of $SnSe_2$ (weight loss: found 64%, calcd. 69.6%) which further decomposes to tin metal finally.

Preparation and characterization of tin selenide nanostructures

Tin selenides nanostructures were prepared by employing **2, 3** and **4** (the chloro complexes have not been used due to their tendency to either volatilize completely or decompose to tin metal (TG analysis), while [$^tBu_2Sn\{SeC_4H(Me\text{-}4,6)_2N_2\}_2$] (**4**) was used for deposition of thin films by AACVD. The resulting products were characterized by solid state diffuse reflectance, thermo gravimetric analysis,

powder X-ray powder diffraction (PXRD), energy dispersive X-ray analysis (EDX), SEM, TEM and selective area electron diffraction (SAED) techniques.

Preparation of tin selenide nano-sheets

Tin selenide nanosheets were synthesized by hot injection of $[R_2Sn\{SeC_4H(Me\text{-}4,6)_2N_2\}_2]$ [R = Et (**2**), ^{n}Bu (**3**) or ^{t}Bu (**4**)] in oleylamine (OLA). Selection of high boiling long chain alkylamine as a surfactant is based on three factors: (i) high boiling point of the amine ensures that the temperature can be raised sufficiently high for decomposition of the single source precursor, (ii) affinity of amines to coordinate with tin and (iii) long chain prevents growth and agglomeration of the nanostructures due to steric hindrance. In a typical experiment, a pale yellow solution of the complex in OLA is injected into hot OLA which quickly changed to different colors ranging from yellow to red to black. After the desired growth time, the reaction was cooled rapidly and toluene (4 ml) was added. The pure black powder was obtained by addition of methanol followed by centrifugation.

Characterization of tin selenide nanostructures

Thermolysis experiments of **2**, **3** and **4** (100 mg each) in OLA (10 ml) for 2, 5 and 10 minutes, respectively at 210 ^{o}C gave black residue of tin selenides. The XRD profiles (Figure 3) of the residues obtained by thermolysis for 2 minutes of **2** and **4** showed a set of reflections originating from (009), (104), (109), (1018), (0027), (0028), (111), (119), (1113), (0033), (209) (for thermolysis of **2**); (009), (109), (1018), (111), (119), (1113), (209) (for thermolysis of **4**) planes of hexagonal phase of $SnSe_2$ (JCPDS File No. 40-1465) corroborated by elemental composition analysis by EDX [from **2**: Sn:Se atom ratio is 31.6:68.4 or 1:2.2 and from **4**: Sn:Se atom ratio is 30.9: 69.1 or 1:2.2]. Similar pattern [Brag reflections (009), (101), (108), (109), (1018), (1019), (0027), (1022), (110), (119), (209)] was observed for a product obtained from thermolysis of **3** and was assigned for hexagonal $SnSe_2$. However, the XRD pattern displayed an additional peak at $2\theta = 23.5^{o}$ which may be assigned to selenium impurity. The intensity of these Brag reflections indicates their crystalline nature. The intensity of reflection from (009) plane indicates that structures has a preferential orientation in [001] direction. Such type of highly oriented 2D nanostructures is previously reported[36]. Similar Bragg's reflections with different lattice parameters (Supplementary information, Table S3) were noted for the residues obtained from **2-4** by thermolysis carried out for 5 and 10 minutes (Supplementary information, Figures S7 and S8).

SEM images (Figure 4, S9) of these residues revealed sheet like structures having smooth and rough edges. The residues obtained by thermolysis of **2** displayed sheets which are uniformly distributed and have rough edges (Figure 4a). The magnified image in the inset showed that the sheets have thickness

in the range of 10-20 nm. SEM micrographs of the residues afforded by thermolysis of **3** revealed sharp edged sheets.

Transmission electron microscopy has been used to find the morphology and phase of the residues. TEM image of the residue obtained by thermolysis of **2** showed needle like structures (Figure 5) which are rolled forms of the sheets. The rolling of sheets happens due to the use of solvent during the preparation of TEM samples because of surface tension. The corresponding SAED pattern exhibit set of lattice planes, (0010), (1021) and (1031) related to hexagonal phase of $SnSe_2$ (JCPDS File No. 40-1465). The spot like pattern indicate single crystalline nature of the rolled sheets. TEM image of the residue obtained by thermolysis of **4** revealed sheets like structures having the boundaries in sub micron range (other than thickness of sheets) and sharp needle like structures which are formed due to the rolling of the nano-sheets (Inset of Figure 6a). Individual nanosheets were also observed in addition to the rolled sheets. HRTEM image of the sheets showed lattice plane with interplanar distance of 6.20 Å corresponding to (009) plane of hexagonal phase of $SnSe_2$ (JCPDS File No. 40-1465) (Figure 6b).

Preparation and characterization of tin selenide thin films

One of the complexes, $[^tBu_2Sn\{SeC_4H(Me\text{-}4,6)_2N_2\}_2]$ (**4**) was employed for deposition of $SnSe_2$ thin film as ^tBu is a good leaving group. Black tin selenide thin films were deposited on p-type silicon (110) substrate using toluene solution of **4** at 375 ^oC for 1 h. There was no deposition below 375 ^oC while very poor coverage at 400 ^oC and above. XRD pattern of as prepared thin films (Figure S10) deposited at 375 ^oC for 1 h showed peaks at 2θ = 25.8, 30.7, 33.9, 37.9, 41.2, 43.4, 47.7, 49.7, 51.8, 54.3 and 57.8^o which may be assigned to the reflections from (0016), (109), (0021), (1016), (1019), (1021), (111), (1025), (1112), (1115) and (209) planes of hexagonal phase of $SnSe_2$ (JCPDS File No. 40-1465). This film annealed at 375 ^oC for 1 h showed XRD reflections (Figure 7) from (009), (100), (109), (0021), (1016), (1021), (110), (1112), (0033) and (2010) planes of hexagonal $SnSe_2$ (JCPDS File No. 40-1465). The composition is further confirmed by EDX analysis (for as prepared thin film: Sn:Se atom ratio is 36.9:63.1 or 1:1.7; for annealed prepared thin film: Sn:Se atom ratio is 38.4:61.6 or 1:1.6). The lattice parameters for as prepared and annealed thin films are a = 3.811(0), c = 55.36(36) Å (as prepared thin films) and a = 3.811(0), c = 55.05(3) Å (annealed thin films), respectively which are in accord with the hexagonal $SnSe_2$ (JCPDS-40-1465). SEM micrographs (Figure 8) of as prepared thin films revealed irregular morphology. However, the annealed thin films revealed hierarchical flower like structures with an average size of ~15 μm.

Optical properties of $SnSe_2$ nanostructures and thin films

Optical properties of $SnSe_2$ nanostructures were investigated using solid state diffuse reflectance spectroscopy. Kubelka-Munk transformations were performed on solid state diffuse reflectance data to determine the optical direct and indirect band gaps. The band gap values were obtained by extrapolating the absorption onsets to the intersection point of the baseline. The plots of $[F(R)h\nu]^2$ versus hν and $[F(R)h\nu]^{1/2}$ versus hν were used to obtain direct and indirect band gaps, respectively.

The direct and indirect band gaps of the nanosheets obtained by thermolysis of **2** and **4** in OLA at 210 ^oC for 2, 5 and 10 minutes showed a gradual decrease from 2.22 to 1.82 (direct band gaps) (Supplementary Figure S11), 1.49 to 1.38 eV (indirect band gaps) (for nanosheets obtained from **2**) (Supplementary Figure S12) and 2.30 to 1.76 (direct band gaps) (Figure 9), 1.48 to 1.46 eV (indirect band gaps) (for nanosheets obtained from **4**) (Supplementary Figure S13) with the increase in reaction time. A blue shift in band gaps was observed for the nanosheets with respect to bulk $SnSe_2$ [E_g (direct) = 1.62 eV and E_g (indirect) = 0.97 eV)][37]. The gradual increase in the band gap values with decreasing thickness of sheets may be either due to quantum confinement or surface effect of the carriers or lattice distortions or surface lattice defects[38]. Since the thickness of the sheets obtained by thermolysis of **2** and **4** in OLA for 2 minutes are in the range of 10-20 nm and there is systematic increase of band gap with decreasing thickness of sheets, quantum confinement may not be ruled out. Band gap values of 1.67-1.62 eV with crystallite size of 31.2-111.4 nm were reported for thin films of $SnSe_2$deposited at substrate temperatures of 150-300 ^oC.[39] The former values when compared with the direct band gap values of 2.22 and 2.30 eV obtained for $SnSe_2$nanosheets in the present investigation indicate that these measured values are justified for the sheets of thickness varying between 10-20 nm. However, the direct band gap values between 2.10 to 1.62 were reported as direct allowed transitions while indirect band gap energies in the range of 0.99-1.3 eV for bulk $SnSe_2$.[37,40-42] The direct[40,42] and indirect band gap[41] values estimated in the present investigation are in the range of reported values.

Similarly, the direct and indirect band gap values for as-deposited $SnSe_2$ thin films obtained by AACVD of [$^tBu_2Sn\{SeC_4H(Me\text{-}4,6)_2N_2\}_2$] (**4**) on silicon substrate at 375 ^oC for 1 h and annealed thin films are 2.12 and 2.06 eV (direct band gap) (Figure 10) and 1.54 and 1.50 eV (indirect band gap) (Supplementary Figure S14), respectively. The obtained direct and indirect band gap values for $SnSe_2$ thin films are comparable to that of literature values[42, 43]. The band gap values correspond to direct and indirect allowed transitions. The decrease in the band gaps for annealed thin films compared to as-deposited thin films may be accounted for thermal expansion of the lattice and temperature dependent electron-phonon interactions[39]. Similar trend in band gap values has been observed for the annealed thin

films with respect to readily deposited thin films in the literature.[42,43] Although the deposition and annealed temperatures are same, the total residence time in the furnace is different. As-deposited thin films are placed in furnace for 1 h during deposition while annealed thin films are obtained after heating the as-deposited thin films at 375°C for additional one hour after their deposition. Table 4 gives a comparison of the band gap values reported in the present investigation with the literature values.[42-44]

Conclusion

Diorganotin(IV) pyrimidyl selenolates complexes have been conveniently synthesized and isolated as air stable monomeric complexes. The complexes, $[R_2Sn\{SeC_4H(Me\text{-}4,6)_2N_2\}_2]$ (R = Et, ^{n}Bu or ^{t}Bu) were used as single source molecular precursors for the preparation of phase pure $SnSe_2$ nano-sheets while thin films were deposited using $[^tBu_2Sn\{SeC_4H(Me\text{-}4,6)_2N_2\}_2]$ by AACVD. The thickness of the nano sheets are in the range of 10-20 nm. The band gap of nano-sheets varies from 1.7 to 2.3 eV (direct band gaps) and 1.49 to 1.36 eV (indirect band gaps) while the direct and indirect band gaps of thin films are in the range of 2.06-2.12 and 1.50-1.54 eV, respectively. These band gaps are blue shifted relative to bulk $SnSe_2$ and gradually increases with decrease in the thickness.

Acknowledgements

We thank Dr. B. N. Jagatap for encouragement of this work. We are grateful to Head, Analytical Chemistry Division and (Mrs.) N. Raje for providing thermo gravimetric analyses data.

Supporting Information

CCDC-Nos. 1420614 to 1420616 for $[^nBu_2Sn\{SeC_4H(Me\text{-}4,6)_2N_2\}_2]$ (**3**), $[^tBu_2Sn\{SeC_4H(Me\text{-}4,6)_2N_2\}_2]$ (**4**), and $[^tBu_2Sn\{SeC_4H(Me\text{-}4,6)_2N_2\}Cl]$ (**7**), respectively contain the supplementary crystallographic data for this paper. These data can be obtained free of charge at www.ccdc.cam.ac.uk/conts/retrieving.html or from the Cambridge Crystallographic Data Centre, 12 Union Road, Cambridge CB2 1EZ, UK [Fax: + 44-1223/336-033; E-mail: deposit@ccdc.cam.ac.uk].

References

1. M. V. Kovalenko, W. Heiss, E. V. Shevchenko, J. S. Lee, H. Schwinghammer, A. P. Alivisatos and D. V. Talapin, *J. Am. Chem. Soc.,* 129 (2007) 11354-11355

2. M. A. Franzman, C.W. Schlenker, M. E. Thompson and R. L. Brutchey, *J. Am. Chem. Soc.*, 132 (2010) 4060-4061.
3. Y. Zhang, J. Lu, S. Shen, H. Xu, and Q. Wang, *Chem. Commun.*, 47 (2011) 5226-5228; C. Zhai, N. Du, and H. Z. D. Yang, *Chem. Commun*., 47 (2011) 1270-1272.
4. J. Choi, J. Jin, J. G. Jung, J. M. Kim, H. J. Kim and S. U. Son, *Chem. Commun*., 47 (2011) 5241-5243; .
5. S. Wen, H. Pan and Y. Zheng, *J. Mater. Chem. C*, 3 (2015) 3714-3721.
6. R. Xie, M. Rutherford and X. Peng, *J. Am. Chem. Soc*., 131 (2009) 5691-5697; D.B. Mitzi, L.L. Kosbar, C.E. Murray, M. Copel and A. Afzall, *Nature*, 428 (2004) 299-303.
7. P. D. Antunez, J. J. Buckley and R. L. Brutchey, *Nanoscale*, 3 (2011) 2399-2411.
8. H. Zhang and D. V. Talapin, *Angew. Chem. Int. Ed.*, 53 (2014) 9126-9127.
9. L. D. Zhao, S. H. Lo, Y. Zhang, H. Sun, G. Tan, C. Uher, C. Wolverton, V. P. Dravid and M. G. Kanatzidis, *Nature*, 508 (2014) 373-377.
10. N. D. Boscher, C. J. Carmalt, R. G. Palgrave and I. P. Parkin, *Thin Solid Films*, 516 (2008) 4750-4757.
11. D. D. Vaughn II, Sn-II In and R. E. Schaak, *ACS Nano*, 5 (2011) 8852-8860.
12. K. Liu, H. Liu, J. Wang and L. Feng, *Materials Lett*., 63 (2009) 512-514.
13. P. Boudjouk, D. J. Seidler, D. Grier and G. J. McCarthy, *Chem. Mater.*, 8 (1996) 1189-1196.
14. P. Boudjouk, D. J. Seidler, S.R. bahr and G. J. McCarthy, *Chem. Mater*., 6 (1994) 2108-2112.
15. S. R. Bahr, P. Boudjouk and G. J. McCarthy, *Chem. Mater.*, 4 (1992) 383-388.
16. I. S. Chuprakov, K. H. Dahmen, J. J. Schneider and J. Hagen, *Chem. Mater.*, 10 (1998) 3467-3470.
17. Y. Cheng, T. J. Emge and J. G. Brennan, *Inorg. Chem*., 35 (1996) 342-346.
18. R. K. Sharma, G. Kedarnath, A. Wadawale, C. A. Betty, B. Vishwanadh and V. K. Jain, *Dalton Trans.*, 41(2012) 12129-12138; J. Otera, T. Yano and K. Kusakabe, Bull. Chem. Soc. Jpn., 56 (1983) 1057–1059.
19. R. S. Chauhan, R. K. Sharma, G. Kedarnath, D. B. Cordes, A. M. Z. Slawin, V. K. Jain, *J. Organomet. Chem.*, 717 (2012) 180-186.
20. B. Philips-Invernizzi, D. Dupont and C. Caze, *Opt. Eng.*, 40 (2001) 1082-1092.
21. T. Higashi, ABSCOR-Empirical Absorption Correction based on Fourier Series Approximation, Rigaku Corporation, 3-9-12 Matsubara, Akishima, Japan, 1995.
22. G. M. Sheldrick, SHELX 97-Program for Crystal Structure Analysis, Göttingen, Germany, 1997; G. M. Sheldrick, *Acta. Crystallogr. A*, 64 (2008) 112.

23. C. K. Johnson, ORTEP II, Report ORNL-5136, Oak Ridge National Laboratory, Oak Ridge TN, 1976.
24. A. Tyagi, G. Kedarnath, A. Wadawale, V. K. Jain, M. Kumar and B. Vishwanadh, *RSC Advances*, 5 (2015) 62882-62890.
25. T. A. K. Al-Allaf, *J. Organomet. Chem.*, 306 (1986) 337-346.
26. P. J. Smith and A. P. Tupciauskas, *Annual Reports on NMR on Spectroscopy*, 8 (1978) 291-370; R. Hani and R. A. Geanangel, *Coord. Chem. Res.*, 44 (1982) 229-246.
27. S. Singh, S. Bhattacharya and H. Nöth, *Eur. J. Inorg. Chem.*, (2010) 5691-5699.
28. A. Eichhöfer, J. J. Jiang, H. Sommer, F. Weigend, O. Fuhr, D. Fenske, C. Y. Su and G. Buth, *Eur. J. Inorg. Chem.*, 2010, 410-418.
29. G. Domazetis, B. D. James, M. F. Mackay and R. J. Magee, *J. Inorg. Nucl. Chem.*, 41 (1979) 1555-1560.
30. V. B. Mokal, V. K. Jain and E. R. T. Tiekink, *J. Organomet. Chem*. 471 (1994) 53-61.
31. A. Bondi, *J. Phys. Chem.*, 18 (1964) 441-452.
32. R. Schmiedgen, F. Huber, H. Preut, G. Ruisi and R. Barbieri, *Appl. Organomet. Chem.*, 8 (1994) 397-407.
33. M. Bouâlam, J. Meunier-Piret, M. Biesemans, R. Willem and M. Gielen, *Inorg. Chim. Acta*, 198-200 (1992) 249-255.
34. S. D. Reid, A. L. Hector, W. Levason, G. Reid, B. J. Waller and M. Webster, *Dalton Trans.*, (2007) 4769-4777.
35. P. Kevin, D. J. Lewis, J. Raftery, M. A. Malik, P. O'Brien, *J. Cryst. Growth,* 415 (2015) 93-99.
36. Z. Fang, S. Hao, L. Long, H. Fang, T. Qiang and Y. Song, *Cryst. Eng. Commun.*, 16 (2014) 2404-2410.
37. G. Dmingo, R. S. Itoga and C. R. Kannewurf, *Phys. Rev.*, 143 (1966) 536-541.
38. M. X. Wang, G. H. Yue1, Y. D. Lin, X. Wen, D. L. Peng and Z. R. Geng, *Nano-Micro Lett.*, 5 (2013) 1.
39. R. Sachdeva, M. Sharma, A. Devi, U. Parihar, N. Kumar, N. Padha and C. J. Panchal, *J. Nano-electron. Phys.*, 3 (2011) 507-513.
40. A. K. Garg, O. P. Agnihotri, A. K. Jain and R. C. Tyagi, *J. Appl. Phys*., 47 (1976) 997-1000.
41. B. L. Evans and R. A. Hazelwood, *J. Phys. D: Appl. Phys*., 2 (1969) 1507-1516.
42. M. M. El-Nahass, *J. Mater. Science*, 27 (1992) 6597-6604.
43. V. P. Bhatt, K. Gireesan and C. F. Desai, *Cryst. Res. Technol.*, 25 (1990) 209.
44. D. Martínez-Escobar, Manoj Ramachandran, A. Sánchez-Juárez and J. S. N. Rios, *Thin Solid Films*, 535 (2013) 390-393.

Table 1. Crystallographic and structural determination data for [^{t}Bu$_2$Sn{SeC$_4$H(Me-4,6)$_2$N$_2$}$_2$] (**4**) and [^{t}Bu$_2$Sn{SeC$_4$H(Me-4,6)$_2$N$_2$}Cl] (**7**).

	[^{t}Bu$_2$Sn{SeC$_4$H(Me-4,6)$_2$N$_2$}$_2$] (**4**)	[^{t}Bu$_2$Sn{SeC$_4$H(Me-4,6)$_2$N$_2$}Cl] (**7**)
Chemical formula	$C_{20}H_{32}N_4Se_2Sn$	$C_{14}H_{25}ClN_2SeSn$
Formula weight	605.11	454.46
Crystal size/mm^3	0.20 × 0.20× 0.10	0.10× 0.05 × 0.05
Crystal system / space group	Monoclinic /C2/*c*	Monoclinic/P2$_1$/*c*
Unit cell dimensions		
a/Å	14.800(4)	9.192(3)
b/Å	7.7490(7)	12.655(3)
c/Å	21.526(4)	15.9900(18)
α	90.00	90.00
β	95.420(17)	92.278(19)
γ	90.00	90.00
Volume/Å^3	2457.7(8)	1858.6(8)
Z	4	4
D_c/g cm^{-3}	1.635	1.624
μ/mm^{-1}	4.013	3.468
F(000)	1192	896
Limiting indices	$-19 \le h \le 10$	$-11 \le h \le 11$
	$0 \le k \le 10$	$-9 \le k \le 16$
	$-27 \le l \le 27$	$-11 \le l \le 20$
No. of reflections collected / unique	2813/ 2067	4261/1963
No. of data / restraints / parameters	2813/ 0/ 128	4261/0/ 181
Final R_1, ωR_2 indices $[I > 2\sigma(I)]$	0.0342, 0.0823	0.0482/0.1019
R_1, ωR_2 (all data)	0.0636, 0.0922	0.1745/0.1485
Goodness of fit on F^2	1.044	1.016

Table 2. Bond lengths (Å) and angles (°) for [^{t}Bu$_2$Sn{SeC$_4$H(Me-4,6)$_2$N$_2$}$_2$] (**4**)

Sn1– Se1	2.5800(6)	Sn1– N1	3.234(4)
Sn1– C7	2.205(4)	Se1– C1	1.910(4)
C7– Sn1–C7^{i}	125.6(2)	Sn1– Se1–C1	98.4(2)
C7–Sn1–Se1	108.3(1)	N1^{i}– Sn1–N1	161.85
C7–Sn1–Se1^{i}	110.7(1)	Se1^{i}– Sn1–Se1	86.19(3)
C7^{i}–Sn1–Se1	110.7(1)		
C7^{i}–Sn1–Se1^{i}	108.3(1)		

Table 3. Bond lengths (Å) and angles (°) for [$^{t}Bu_2Sn\{SeC_4H(Me\text{-}4,6)_2N_2\}Cl$] (**7**)

Sn1–C7	2.21	Sn1–Se1	2.545(1)
Sn1– C11	2.19(1)	Sn1– N1	2.784(7)
Sn1– Cl1	2.418(3)	Se1– C1	1.887(9)
C7–Sn1– C11	126.7(4)	C11– Sn1– Cl1	97.2(3)
C7–Sn1– Cl1	98.1(3)	C11– Sn1– N1	95.7(3)
C7–Sn1– Se1	115.7(3)	Cl1– Sn1– Se1	92.1(9)
C7–Sn1– N1	91.9(3)	Se1–Sn1– N1	62.6(2)
C11–Sn1– Se1	114.4(3)	Cl1–Sn1– N1	154.1(2)
Cl1– Sn1– Se1	92.10(9)		

Table 4. Band gap values for $SnSe_2$ thin films at room temperature.

Method	Deposition Temperature (^oC)/ Crystalline state	Direct band gap (eV)	Indirect band gap (eV)	Reference
AACVD of [$^tBu_2Sn\{SeC_4H(Me\text{-}4,6)_2N_2\}_2$] (**4**)	375/ As prepared crystalline thin film	2.12	1.54	Present work
AACVD of [$^tBu_2Sn\{SeC_4H(Me\text{-}4,6)_2N_2\}_2$] (**4**)	375/ Annealed crystalline thin film	2.06	1.50	Present work
Thermal evaporation of $SnSe_2$	27/ Amorphous	2.05	0.99	42
Thermal evaporation of $SnSe_2$	300/ Crystalline	2.02	0.95	42
Thermal evaporation of $SnSe_2$	-/ As deposited thin film	1.62	1.42	43
Thermal evaporation of $SnSe_2$	200/ Annealed thin film	1.43	1.24	43
Spray pyrolysis of $SnCl_2{\cdot}2H_2O$ and 1,1-dimethyl-2-selenourea	300/ Crystalline	1.48	-	44
Spray pyrolysis of $SnCl_2{\cdot}2H_2O$ and 1,1-dimethyl-2-selenourea ($C_3H_8N_2Se$)	350/ Crystalline	1.59	-	44

Figure Captions:

Fig. 1 Crystal structure of [$^{t}Bu_2Sn\{SeC_4H(Me\text{-}4,6)_2N_2\}_2$] (**4**) with atomic number scheme. The ellipsoids were drawn at 50% probability.

Fig. 2 Crystal structure of [$^{t}Bu_2Sn\{SeC_4H(Me\text{-}4,6)_2N_2\}Cl$] (**7**) with atomic number scheme. The ellipsoids were drawn at 25% probability.

Fig. 3 a) Simulated XRD pattern of hexagonal $SnSe_2$ (JCPDS-40-1465). XRD profiles of $SnSe_2$ nanosheets obtained by b) thermolysis of [$Et_2Sn\{SeC_4H(Me\text{-}4,6)_2N_2\}_2$] (**2**), c) [$^{n}Bu_2Sn\{SeC_4H(Me\text{-}4,6)_2N_2\}_2$] (**3**) and d) [$^{t}Bu_2Sn\{SeC_4H(Me\text{-}4,6)_2N_2\}_2$] (**4**) in OLA at 210 ^{o}C for 2 minutes ('*' indicates the impurity peak of Se). Simulated pattern has been avoided for clarity.

Fig. 4 SEM images of $SnSe_2$ nanosheets obtained by a) thermolysis of [$Et_2Sn\{SeC_4H(Me\text{-}4,6)_2N_2\}_2$] (**2**), b) [$^{n}Bu_2Sn\{SeC_4H(Me\text{-}4,6)_2N_2\}_2$] (**3**) and c) [$^{t}Bu_2Sn\{SeC_4H(Me\text{-}4,6)_2N_2\}_2$] (**4**) in OLA at 210 ^{o}C for 2 minutes (Inset show magnified images of the same).

Fig. 5 a) TEM image and b) SAED pattern of $SnSe_2$ nanosheets obtained by thermolysis of [$Et_2Sn\{SeC_4H(Me\text{-}4,6)_2N_2\}_2$] (**2**) in OLA at 210 ^{o}C for 2 minutes.

Fig. 6 a) TEM image and b) HRTEM pattern of $SnSe_2$ nanosheets obtained by thermolysis of [$^{t}Bu_2Sn\{SeC_4H(Me\text{-}4,6)_2N_2\}_2$] (**4**) in OLA at 210 ^{o}C for 2 minutes (Inset show needle like structures formed by rolling of nanosheets).

Fig. 7 XRD profile of $SnSe_2$ thin film obtained by AACVD of [$^{t}Bu_2Sn\{SeC_4H(Me\text{-}4,6)_2N_2\}_2$] (**4**) on silicon substrate at 375 ^{o}C for 1 h followed by annealing at the same temperature for 1 h overlaid on simulated XRD pattern of hexagonal $SnSe_2$ (JCPDS-40-1465).

Fig. 8 SEM images of a) as prepared $SnSe_2$ thins films obtained by AACVD of [$^{t}Bu_2Sn\{SeC_4H(Me\text{-}4,6)_2N_2\}_2$] (**4**) on silicon substrate at 375 ^{o}C for 1 h and b) annealed thin film of as prepared thin film at 375 ^{o}C for 1 h.

Fig. 9 Plots of $[F(R)h\nu]^2$ vs energy generated by Kubelka-Munk transformation of solid-state diffuse reflectance data of $SnSe_2$ nano-sheets obtained by thermolysis of [$^{t}Bu_2Sn\{SeC_4H(Me\text{-}4,6)_2N_2\}_2$] (**4**) in OLA at 210 ^{o}C for a) 2, b) 5 and c) 10 minutes, respectively for determining direct band gap energies.

Fig. 10 Plots of $[F(R)h\nu]^2$ vs energy generated by Kubelka-Munk transformation of solid-state diffuse reflectance data of a) as-deposited $SnSe_2$ thin films obtained by AACVD of [$^{t}Bu_2Sn\{SeC_4H(Me\text{-}4,6)_2N_2\}_2$] (**4**) on silicon substrate at 375 ^{o}C for 1 h and b) annealed thin films to determine direct band gap energies.

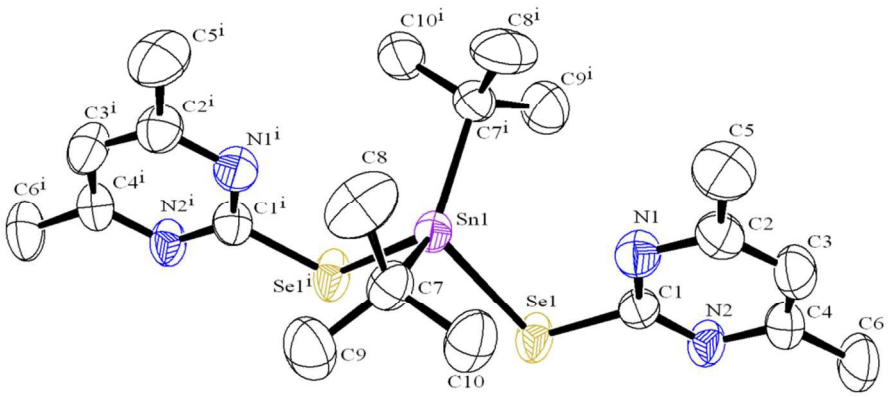

Fig. 1 Crystal structure of [$^{t}Bu_2Sn\{SeC_4H(Me\text{-}4,6)_2N_2\}_2$] (**4**) with atomic number scheme. The ellipsoids were drawn at 50% probability.

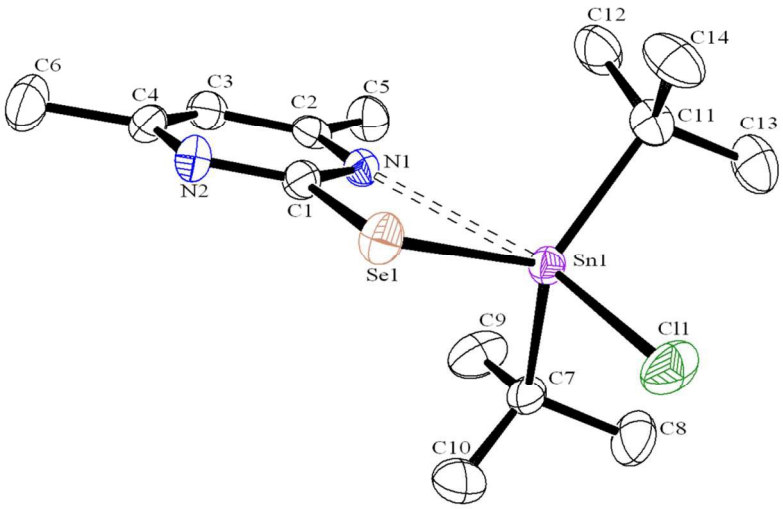

Fig. 2 Crystal structure of [$^{t}Bu_2Sn\{SeC_4H(Me\text{-}4,6)_2N_2\}Cl$] (**7**) with atomic number scheme. The ellipsoids were drawn at 25% probability.

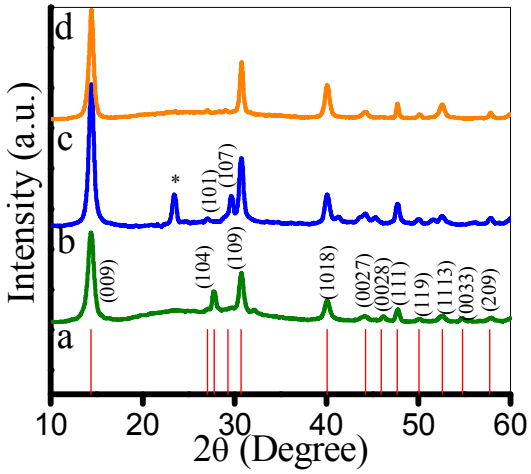

Fig. 3 a) Simulated XRD pattern of hexagonal $SnSe_2$ (JCPDS-40-1465). XRD profiles of $SnSe_2$ nanosheets obtained by b) thermolysis of $[Et_2Sn\{SeC_4H(Me\text{-}4,6)_2N_2\}_2]$ (**2**), c) $[^nBu_2Sn\{SeC_4H(Me\text{-}4,6)_2N_2\}_2]$ (**3**) and d) $[^tBu_2Sn\{SeC_4H(Me\text{-}4,6)_2N_2\}_2]$ (**4**) in OLA at 210 ^oC for 2 minutes ('*' indicates the impurity peak of Se). Simulated pattern has been avoided for clarity.

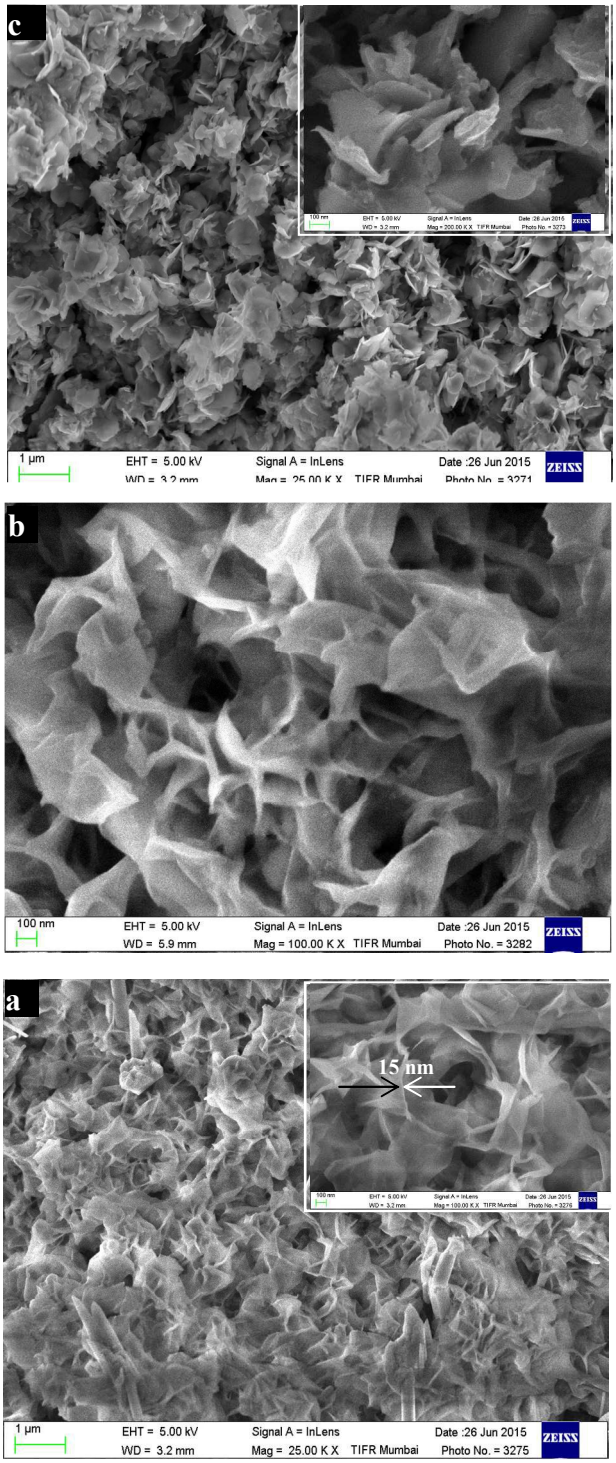

Fig. 4 SEM images of $SnSe_2$ nanosheets obtained by a) thermolysis of $[Et_2Sn\{SeC_4H(Me\text{-}4,6)_2N_2\}_2]$ (**2**), b) $[^nBu_2Sn\{SeC_4H(Me\text{-}4,6)_2N_2\}_2]$ (**3**) and c) $[^tBu_2Sn\{SeC_4H(Me\text{-}4,6)_2N_2\}_2]$ (**4**) in OLA at 210 ^oC for 2 minutes (Inset show magnified images of the same).

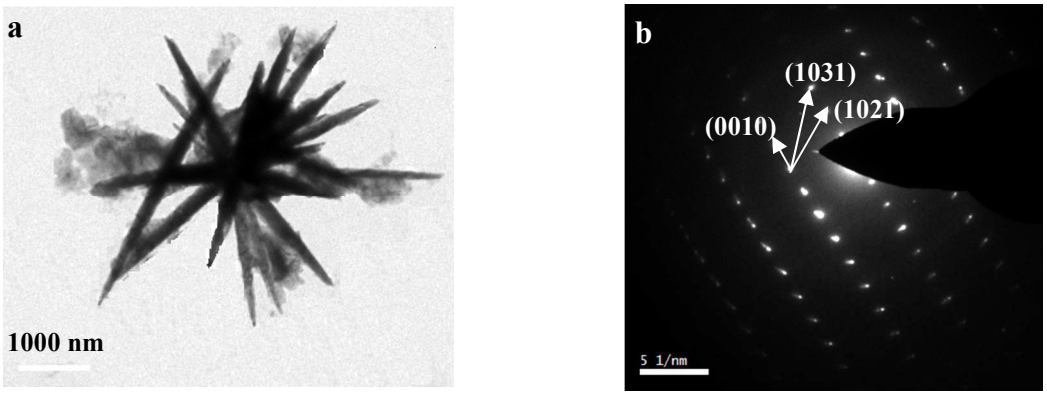

Fig. 5 a) TEM image and b) SAED pattern of $SnSe_2$ nanosheets obtained by thermolysis of $[Et_2Sn\{SeC_4H(Me\text{-}4,6)_2N_2\}_2]$ (**2**) in OLA at 210 ^oC for 2 minutes.

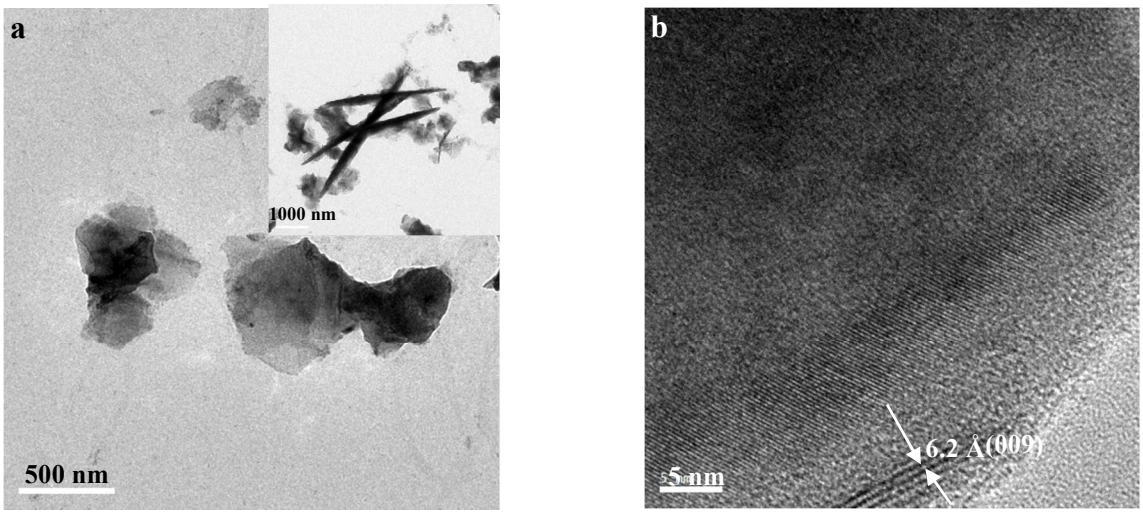

Fig. 6 a) TEM image and b) HRTEM pattern of $SnSe_2$ nanosheets obtained by thermolysis of $[^tBu_2Sn\{SeC_4H(Me\text{-}4,6)_2N_2\}_2]$ (**4**) in OLA at 210 ^oC for 2 minutes (Inset show needle like structures formed by rolling of nanosheets).

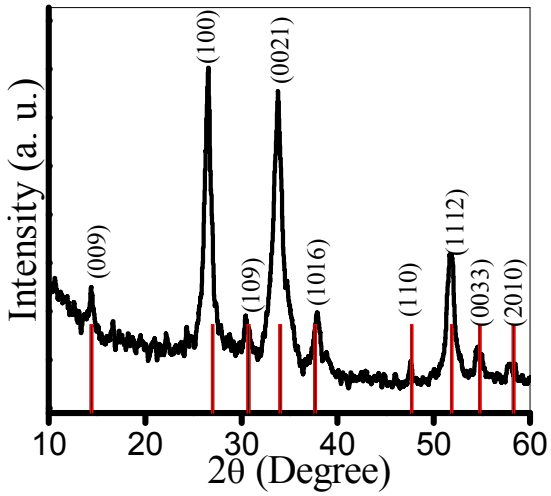

Fig. 7 XRD profile of $SnSe_2$ thin film obtained by AACVD of [$^tBu_2Sn\{SeC_4H(Me\text{-}4,6)_2N_2\}_2$] (**4**) on silicon substrate at 375 ^oC for 1 h followed by annealing at the same temperature for 1 h overlaid on simulated XRD pattern of hexagonal $SnSe_2$ (JCPDS-40-1465).

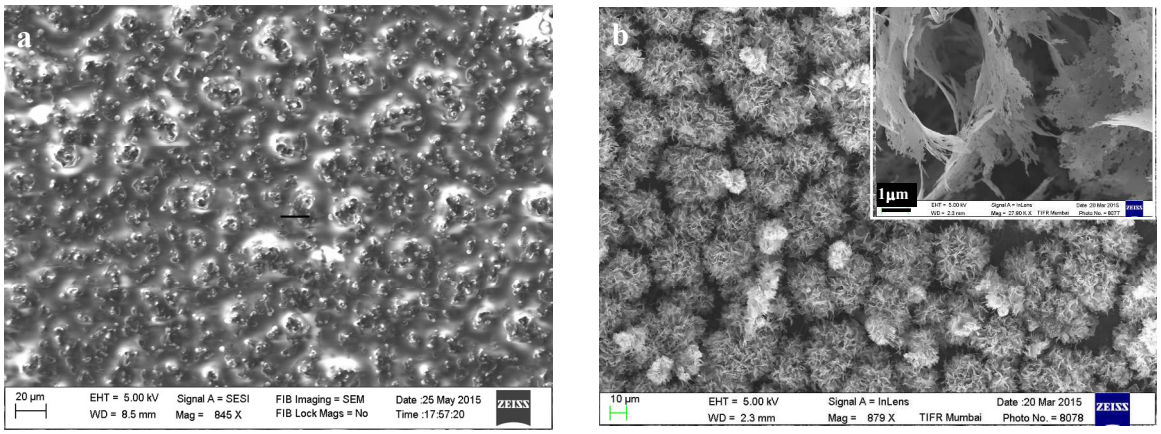

Fig. 8 SEM images of a) as prepared $SnSe_2$ thins films obtained by AACVD of [$^tBu_2Sn\{SeC_4H(Me\text{-}4,6)_2N_2\}_2$] (**4**) on silicon substrate at 375 ^oC for 1 h and b) annealed thin film of as prepared thin film at 375 ^oC for 1 h.

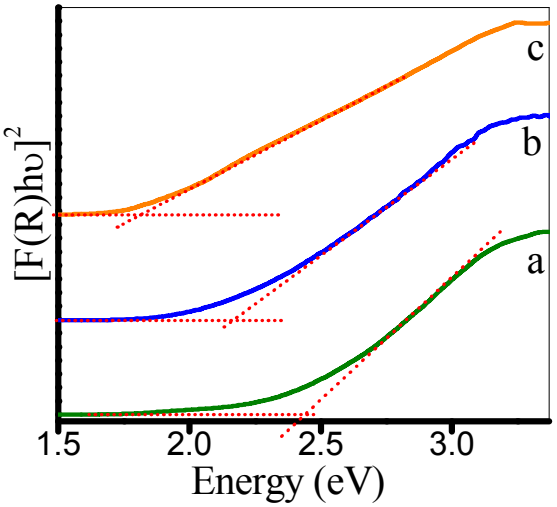

Fig. 9 Plots of $[F(R)h\nu]^2$ vs energy generated by Kubelka-Munk transformation of solid-state diffuse reflectance data of $SnSe_2$ nano-sheets obtained by thermolysis of $[^tBu_2Sn\{SeC_4H(Me\text{-}4,6)_2N_2\}_2]$ (**4**) in OLA at 210 ^oC for a) 2, b) 5 and c) 10 minutes, respectively for determining direct band gap energies.

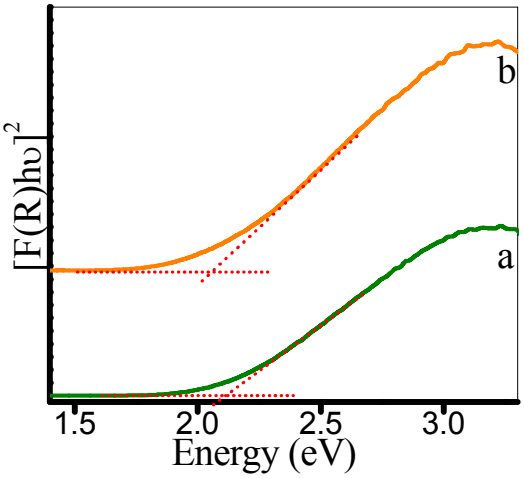

Fig. 10 Plots of $[F(R)h\nu]^2$ vs energy generated by Kubelka-Munk transformation of solid-state diffuse reflectance data of a) as-deposited $SnSe_2$ thin films obtained by AACVD of $[^tBu_2Sn\{SeC_4H(Me\text{-}4,6)_2N_2\}_2]$ (**4**) on silicon substrate at 375 ^oC for 1 h and b) annealed thin films to determine direct band gap energies.

Table of contents

Diorganotin(IV) 4,6-dimethyl-2-pyrimidyl selenolates: Synthesis, structures and their utility as molecular precursors for the preparation of $SnSe_2$ nano-sheets and thin films

Adish Tyagi, G. Kedarnath, Amey Wadawale, Alpa Y Shah, Vimal K. Jain and B. Vishwanadh

Organotin complexes, $[R_2Sn\{SeC_4H(Me\text{-}4,6)_2N_2\}_2]$ and $[R_2SnCl\{SeC_4H(Me\text{-}4,6)_2N_2\}]$ (R = alkyl) were prepared and utilized as ssps for the preparation of $SnSe_2$ nanosheets and thin films. Tunability of band gaps has been demonstrated.